Available online at www.sciencedirect.com
ScienceDirect
Trans. Nonferrous Met. Soc. China 35(2025) 2435−2448
Transactions of Nonferrous Metals Society of China
www.tnmsc.cn

Synergistic effects of Er and Sc on aging behavior and θ' precipitation stability of Al−Cu alloys

Xing-kai HOU[1], Sheng-ping WEN[1], Peng QI[2], Wu WEI[1], Xiao-lan WU[1], Hui HUANG[1], Kun-yuan GAO[1], Xiang-yuan XIONG[1], Zuo-ren NIE[1]

1. Faculty of Materials and Manufacturing, National Engineering Laboratory for Industrial Big-data Application Technology, Beijing University of Technology, Beijing 100124, China;
2. Chinalco Science and Technology Institute Co., Ltd., Beijing 102209, China

Received 15 December 2023; accepted 7 August 2024

Abstract: The effects of the synergistic addition of Er and Sc on the aging and interfacial segregation behaviors of alloys were systematically studied using transmission electron microscopy (TEM) and high-angle annular dark field (HAADF) imaging. The TEM results show that $Al_3(Sc,Zr)$ with a core-shell structure can act as nucleation particles for θ' to promote uniform and fine precipitation. The STEM results show that Er solute atoms were preferentially enriched inside the θ' precipitate during thermal exposure at 225 °C for 150 h. However, Sc and Mn solute atoms segregated at the θ'/α-Al matrix interface were observed at 300 °C. Due to the early enrichment of Er in the θ' precipitate, the slowly diffusing Sc and Mn were segregated to the interface of the θ' precipitate before the severe coarsening of the θ' precipitate, thus further stabilizing the θ' precipitate at higher temperatures.

Key words: Er−Sc co-addition; aging behavior; θ' precipitation stability; solute segregation; Al−Cu alloys

1 Introduction

Precipitation-strengthened Al−Cu alloys are important lightweight engineering materials for applications in the aerospace and automotive industries because of their excellent specific strength ratios and good casting ability [1,2]. The strength of Al−Cu alloys mainly originates from the formation of metastable phases such as θ''/θ' plates with a high number density and high aspect ratio during heat treatment [3−5]. However, at elevated working environment temperatures (~200 °C), the transformation of the θ' phase into the θ-Al_2Cu phase is favored [6,7]. This transformation is accompanied by a loss of strength, which leads to the failure of components such as aircraft skins, fuselages, and wings, as well as automobile engine cylinders, during their service life [8]. Consequently, determining how to improve the stability of the metastable θ' phase at high temperatures is the key to expanding the work temperature range (200−300 °C) of Al−Cu alloys.

In recent years, the segregation of micro-alloyed solutes (such as Mn, Fe, Sc, and Zr [9]) at the Al/θ' interface, which lowers the interfacial energy, has attracted great interest. The segregation of microalloying elements at the θ' interface improves the stability of θ' plate. GAO et al [10] constructed a triple segregation interface structure of Sc−Fe−Si at the θ'/α-Al matrix interface. The thermal stability of θ'-Al_2Cu phases was further optimized by inhibiting interfacial migration. The strongest interfacial Sc segregation leads to the

Corresponding author: Sheng-ping WEN, Tel: +86-13552521441, E-mail: wensp@bjut.edu.cn;
Zuo-ren NIE, Tel: +86-10-67391536, E-mail: zrnie@bjut.edu.cn
https://doi.org/10.1016/S1003-6326(25)66825-7

greatest promotion of θ' precipitation [11]. POPLAWSKY et al [12] found that Mn of Al7CuMnZr alloy was segregated more rapidly to the θ' coherent interface, preventing the migration of the θ' interface. Similar results were reported by SHYAM et al [13] and SUN et al [14]. NIU et al [15] found that Ce atoms could enter the lattice of the θ' precipitates, impeding the movement of interstitial Cu atoms. However, the slow diffusion of Mn and Zr below 300 °C cannot stabilize the θ' plate in time, resulting in rapid deterioration of the mechanical properties of the Al−Cu alloys after long-term aging below 300 °C. Comparatively, the diffusion rates of Er and Sc are faster than that of Mn between 200 and 300 °C. The enrichment of Er in θ' precipitates was observed in Al−Cu−Mg alloys by LIANG et al [16].

Previous studies have shown that the addition of microalloying elements (Sc, Ta, Zr, Nb, and Hf) can form nano-stable $Al_3Sc/Al_3(Sc,Zr)$ [17−19], $(Al,Cu)_3(Zr,Ta)$ [20], Al_3Zr [21], and $(Al,Si)_3Hf$ [22] phases with $L1_2$ structure. The introduction of these nano-precipitated phases is also a feasible method to improve the thermal stability and mechanical properties of Al−Cu alloys. However, Sc is extremely expensive, and the solid solubility of Sc in α-Al matrix is very low, resulting in a limited volume fraction of $Al_3(Sc,Zr)$ precipitates. In fact, this strength effect appears to be even more pronounced when Er is microalloyed with Sc and Zr [23−25]. LIU et al [24] added Er to Al−Sc−Zr alloy and found that Er promoted the nucleation rate of $L1_2$-structured nanoparticles, resulting in a higher density and more homogeneous dispersion. Si and metallic solutes (M) can form M−Si−V clusters (where V is a vacancy), which accelerates the diffusion of isolated M atoms in the fcc-Al matrix [26]. The Si-vacancy clusters may act as heterogeneous nucleation sites to promote the precipitation of Al_3Sc and increase the number density and volume fraction, as observed in Al−Sc−Zr and Al−Sc−Er−Zr alloys [27,28]. The formation of $Al_3(Sc,Zr)$ core/shell dispersions also provides heterogeneous nucleation sites by reducing the energy barrier of θ' nucleation, resulting in fine θ' precipitates to improve the mechanical properties of the Al−Cu alloy [19,29].

To the best of our knowledge, we suspected that Er and Sc could effectively segregate at the θ' plate interface at low temperature or early in the thermal exposure process to improve the room-temperature and high-temperature properties. Therefore, this work aims to study Er and Sc co-addition to further improve the mechanical properties of Al−Cu alloys and stabilize θ' precipitates. Following the heat treatment route designed by MAKINENI et al [21], the hardness during artificial aging at 175 °C and 150 h of thermal exposure at 225 and 300 °C was measured. Combined with TEM and differential correction HAADF imaging, the coarsening process of θ' precipitation and the segregation of specific elements at the θ' interface were quantitatively evaluated. This study will contribute to the development of new Al−Cu materials with solute element segregation at the θ/α-Al interface and provide ideas for new alloy design strategies to further expand the temperature range for the use of Al−Cu alloys.

2 Experimental

The chemical compositions of the experimental Al−Cu alloys are listed in Table 1. The alloys were melted in an electric resistance furnace using high purity aluminum (99.99%Al), Al−10wt.%Mn, Al−20wt.%Si, and Al−50wt.%Cu master alloys at 780 °C. The Al−10wt.%Zr, Al−6wt.%Er and Al−2wt.%Sc master alloys were added at 760 °C after melting. After removing the surface slag, C_2Cl_6 was added to remove the slag and gas, and the mixture stood for 10−15 min

Table 1 Compositions of experimental alloys (wt.%)

Alloy	Cu	Mn	Si	Er	Sc	Zr	Al
Al−4.0Cu−0.2Si	4.24	0.34	0.19	−	−	0.15	Bal.
Al−4.0Cu−0.1Er−0.2Si	4.02	0.32	0.18	0.10	−	0.17	Bal.
Al−4.0Cu−0.1Er−0.1Sc−0.2Si	3.98	0.33	0.19	0.10	0.10	0.18	Bal.
Al−4.0Cu−0.1Sc−0.2Si	3.93	0.34	0.19	−	0.10	0.12	Bal.
Al−4.0Cu−0.1Sc	3.90	−	−	−	0.10	−	Bal.

before being poured into an iron mold. Each of the as-cast alloys was homogenized at 450 °C for 8 h in order to obtain a homogeneous microstructure. The ingot of 30 mm × 15 mm × 150 mm plate was rolled into a plate with a 5 mm (width) × 32 mm (thickness) square cross-section at 450 °C. The rolled alloy sheets were solution treated at (400 °C, 10 h) + (540 °C, 0.5 h), followed by water quenching to room temperature. The water quenched alloy sheets were subjected to aging treatment at 175 °C in an air furnace for time periods ranging from 30 min to 200 h. Some samples aged to peak-hardness at 175 °C were thermally exposed at 225 and 300 °C respectively to study their high-temperature behaviors and the thermal stability.

The hardness was measured by the HXD−1000 Vickers hardness (HV) tester. The loading force was 0.98 N, the holding time was 15 s, and an average value was obtained from 7 test points. The microstructure was observed by TEM and an atomic resolution HAADF-STEM providing Z-contrast images. Twin-jet electrochemical equipment was used for preparing thin discs, and the discs were 3 mm in diameter. The twin-jet equipment was operated at voltage of 12−15 V in a solution composed of 25 vol.% HNO_3 acid and 75 vol.% CH_3OH, and in a temperature condition of −20 °C. TEM and HAADF-STEM observations were performed by transmission electron microscopy of model Cs-corrected Titan-G2 operated at accelerating voltage of ~300 kV with a probe convergence semi-angle of 21.4 mrad and collection semi-angle from 53 to 200 mrad. All the prepared samples were plasma cleaned for 8 min before TEM observation.

3 Results

3.1 Hardness evolution with addition of Er and Sc

Figure 1 presents the hardness evolution during artificial aging at 175 °C for all the tested alloys. The Al−Cu−Er−Sc−Si alloy was found to have almost reached peak hardness (HV ~126.4) after only 6 h at 175 °C. Such a fast aging response rate was not observed for the other alloys. In contrast, it took approximately 12 and 24 h for the Al−Cu−Sc−Si and Al−Cu−Sc alloys to reach peak hardness, respectively. Comparing the Al−Cu−Sc−Si and Al−Cu−Sc alloys, the addition of Si reduced the time required for the Al−Cu−Sc alloy to reach peak hardness and increased the peak hardness by HV ~13.7. After 12 h at 175 °C, the hardness of the Al−Cu−Er−Sc−Si alloy was not significantly different from that of Al−Cu−Sc−Si alloy (HV ~125.8), but it was higher than that of the Al−Cu−Si and Al−Cu−Er−Si alloys. The peak hardness of the Al−Cu−Er−Sc−Si alloy was found to be HV ~28.2 higher than that of the Al−Cu−Si alloy and HV ~21.3 higher than that of the Al−Cu−Er−Si alloys. This condition was selected for the further study of the heat resistance and high-temperature performance of the Al−Cu−Er−Sc−Si alloy. The hardness was observed to continuously decrease for the Al−Cu−Er−Sc−Si and Al−Cu−Sc−Si alloys as the aging time was extended to 200 h, which is a sign of growth and coarsening of the θ' precipitates. However, the hardness of the Al−Cu−Er−Sc−Si alloy decreased only slightly (HV ~14.7). The final hardness remained higher than that of the Al−Cu−Sc−Si alloy, which was approximately HV ~6.2. This indicates further enhancement of the coarsening resistance of the θ' precipitates in the Al−Cu−Sc−Si alloy with the combined addition of Er and Sc.

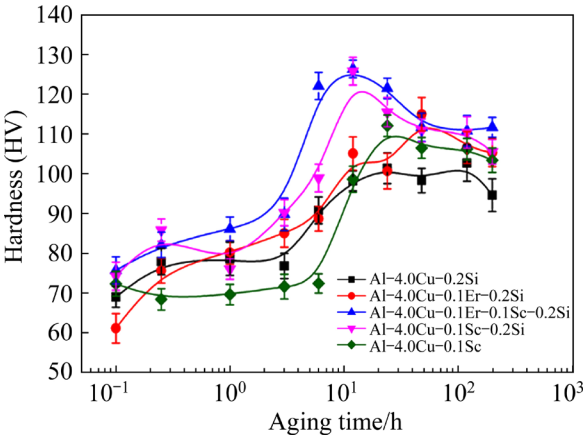

Fig. 1 Hardness evolution of alloys during isothermal aging at 175 °C

Figure 2 shows the hardness curves of the experimental alloys exposed to temperatures of 225 and 300 °C for various time after aging at 175 °C for 12 h. An increase in the hardness of Al−Cu−Er−Si alloys was observed between 0.5 and 3 h during thermal exposure at 225 °C (Fig. 2(a)). This indicated that the hardness of the alloy did not reach its maximum after aging at 175 °C for 12 h, and

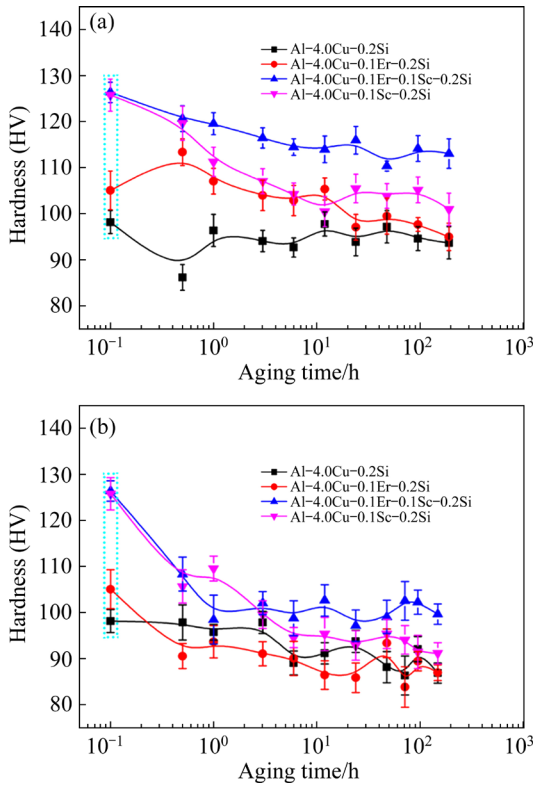

Fig. 2 Hardness evolution curves of alloys aged at 175 °C for 12 h after thermal exposure at 225 °C (a) and 300 °C (b)

θ' precipitates continued to form at 225 °C. The hardness of the Al−Cu−Er−Sc−Si and Al−Cu−Sc−Si alloys decreased obviously in the early stage of thermal exposure, which is a sign of over aging. The combined addition of Er and Sc significantly improves the thermal stability of the Al−Cu alloy. The hardness of the resulting alloy remained relatively stable after aging for 12 h at 225 °C, and its hardness (HV ~114.8) was significantly higher than that of the Al−Cu−Si alloy with only Er or only Sc during long-term thermal exposure for up to 192 h. Compared with the peak hardness, the hardness only decreased by HV ~11.6. Figure 2(b) shows the evolution of hardness as a function of time at 300 °C. The hardness evolution of the Al−Cu−Si alloy shows a similar trend to that during the thermal exposure at 225 °C. However, no increase in hardness was observed in Al−Cu−Si and Al−Cu−Er−Si alloys during thermal exposure at 300 °C, which was related to the rapid growth and coarsening of θ' precipitates at higher temperatures. In summary, the Al−Cu−Er−Sc−Si alloy exhibited both the highest hardness (HV ~99.7) and best stability during thermal exposure. The stabilization effect of the combined addition of Er and Sc in the Al−Cu−Si alloy during thermal exposure is superior to those with only Er or only Sc.

3.2 TEM characterization of microstructure

Al−Cu alloys with added Er and Sc after artificial aging at 175 °C for 12 h were characterized by TEM. Figure 3 shows the θ' precipitate distribution and selected area electron diffraction (SAED) pattern along the $[010]_{Al}$ zone axis in all the studied

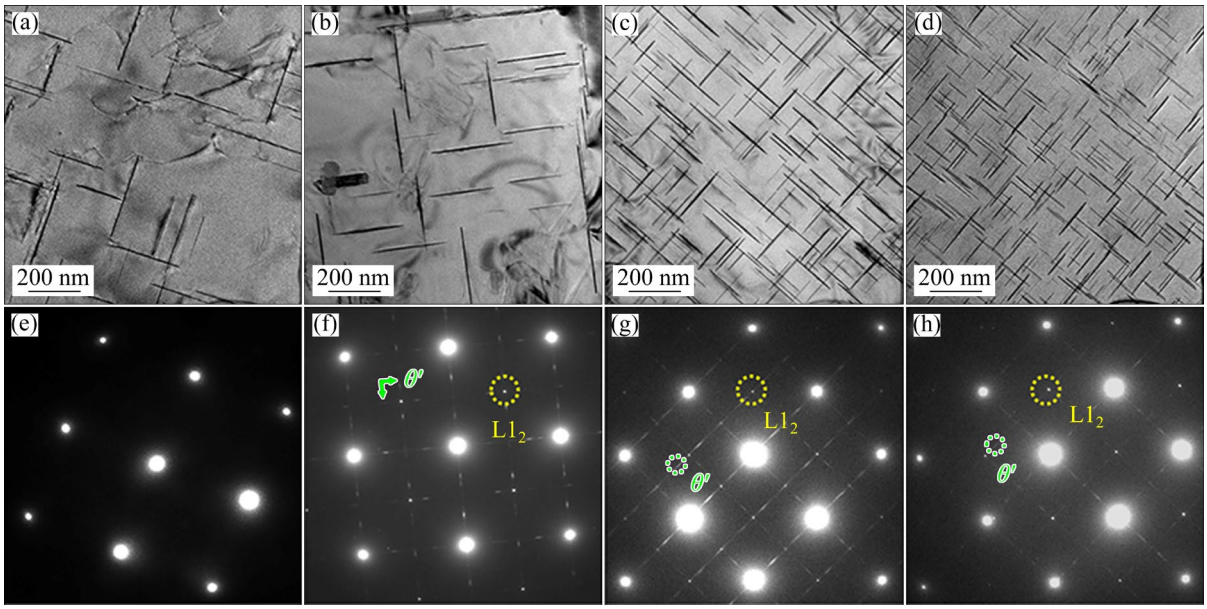

Fig. 3 TEM bright-field images (a−d) and SAED patterns (e−h) along $[010]_{Al}$ zone axis of θ' precipitates in alloys after 12 h of artificial aging at 175 °C: (a, e) Al−Cu−Si; (b, f) Al−Cu−Er−Si; (c, g) Al−Cu−Er−Sc−Si; (d, h) Al−Cu−Sc−Si

alloys. The statistical results for the average length and thickness of the θ' precipitates in the experimental alloys are presented in Table 2. After treatment at 175 °C for 12 h, the diameter of the θ' precipitates in the Al−Cu−Si alloy (249.5 nm) is higher than that in the Al−Cu−Er−Sc−Si (180.1 nm) and Al−Cu−Sc−Si alloys (170.2 nm). Additionally, with the addition of Er and Sc, the number density of θ' precipitates in the Al−Cu−Er−Sc−Si and Al−Cu−Sc alloys increased (Fig. 3(c)), which explains its highest hardness. Figures 3(f−h) show the SAED patterns along the $[010]_{Al}$ zone axis, which all contain superlattice sites corresponding to the $L1_2$ ordering, marked with yellow circles. Further, the additional superlattice spots around the $L1_2$ spots correspond to the θ' phase, which are marked with green circles.

The dark-field TEM images shown in Fig. 4 were obtained from $L1_2$ spot in the SAED pattern. It shows the coexistence of the globular $L1_2$-ordered precipitates and θ' plates. Some of θ' plates nucleate on pre-existing $L1_2$-ordered precipitates in the matrix. In the Al−Cu−Sc−Si alloy, the number density of spherical precipitates was lower than that in the Al−Cu−Er−Sc−Si alloy (Fig. 4(b)). The uniform distribution of fine θ' precipitates with high number density in the Al−Cu−Er−Sc−Si and Al−Cu−Sc−Si alloys is consistent with the refinement of the θ' precipitates as they nucleate on the previously reported $Al_3(Sc,Zr)$ [29] or $Al_3(Er,Sc,Zr)$ dispersions. The statistical results for the average length and thickness of the θ' precipitates in experimental alloys are presented in Table 2.

Table 2 Average length, thickness and aspect ratio of θ' precipitates in alloys treated at 175 °C for 12 h

Alloy	Length/ nm	Thickness/ nm	Aspect ratio
Al−Cu−Si	249.5±65.4	7.0±2.0	35.6
Al−Cu−Er−Si	209.1±82.2	6.5±1.9	32.3
Al−Cu−Er−Sc−Si	180.1±40.2	6.2±2.3	29.3
Al−Cu−Sc−Si	171.3±55.5	6.0±1.5	28.4

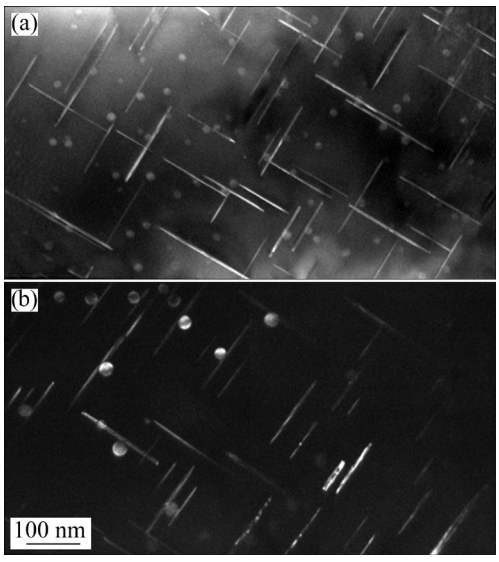

Fig. 4 Dark-field TEM images from $L1_2$ spot in SAED pattern of alloys after being treated at 175 °C for 12 h: (a) Al−Cu−Er−Sc−Si; (b) Al−Cu−Sc−Si

3.3 Microstructural stability of θ' plates

The peak-aged Al−Cu−Si, Al−Cu−Er−Sc−Si and Al−Cu−Sc−Si alloys were exposed to temperatures of 225 and 300 °C for 150 h to evaluate the synergistic effects of the addition of Er and Sc on the stability of the microstructures. Figure 5 shows the corresponding statistical results for the length and thickness of θ' plates and the TEM images after thermal exposure at 225 °C. The coarsening resistance of θ' precipitates at elevated temperatures can be evaluated by the variation in their length, thickness, and number density. Thermal exposure of the peak-aged Al−Cu−Si alloy at 225 °C led to a 30% increase in the length of the θ' precipitates. With the addition of Sc, the length and thickness of the θ' precipitates increased slightly, by 16% and 17%, respectively. This indicates that the growth of θ' precipitates at high temperatures is hindered by the addition of Sc. Obviously, after the combined addition of both Er and Sc to the trinary Al−Cu−Si alloy, the decrease in the number density and the increase in the length and thickness of the plates were the smallest. The average length and thickness of the thermally exposed Al−Cu−Er−Sc−Si alloy were 173.5 and 6.79 nm, respectively. Compared with the parameters of the alloy after peak aging at 175 °C for 12 h, the average thickness was only increased by 10%, which indicates that the main strengthening phase θ' in the Al−Cu−Er−Sc−Si alloy does not coarsen significantly after 225 °C thermal exposure.

After thermal exposure at 300 °C for 150 h, the length and thickness of θ' plates decreased with increasing temperature in the three alloys (Fig. 6).

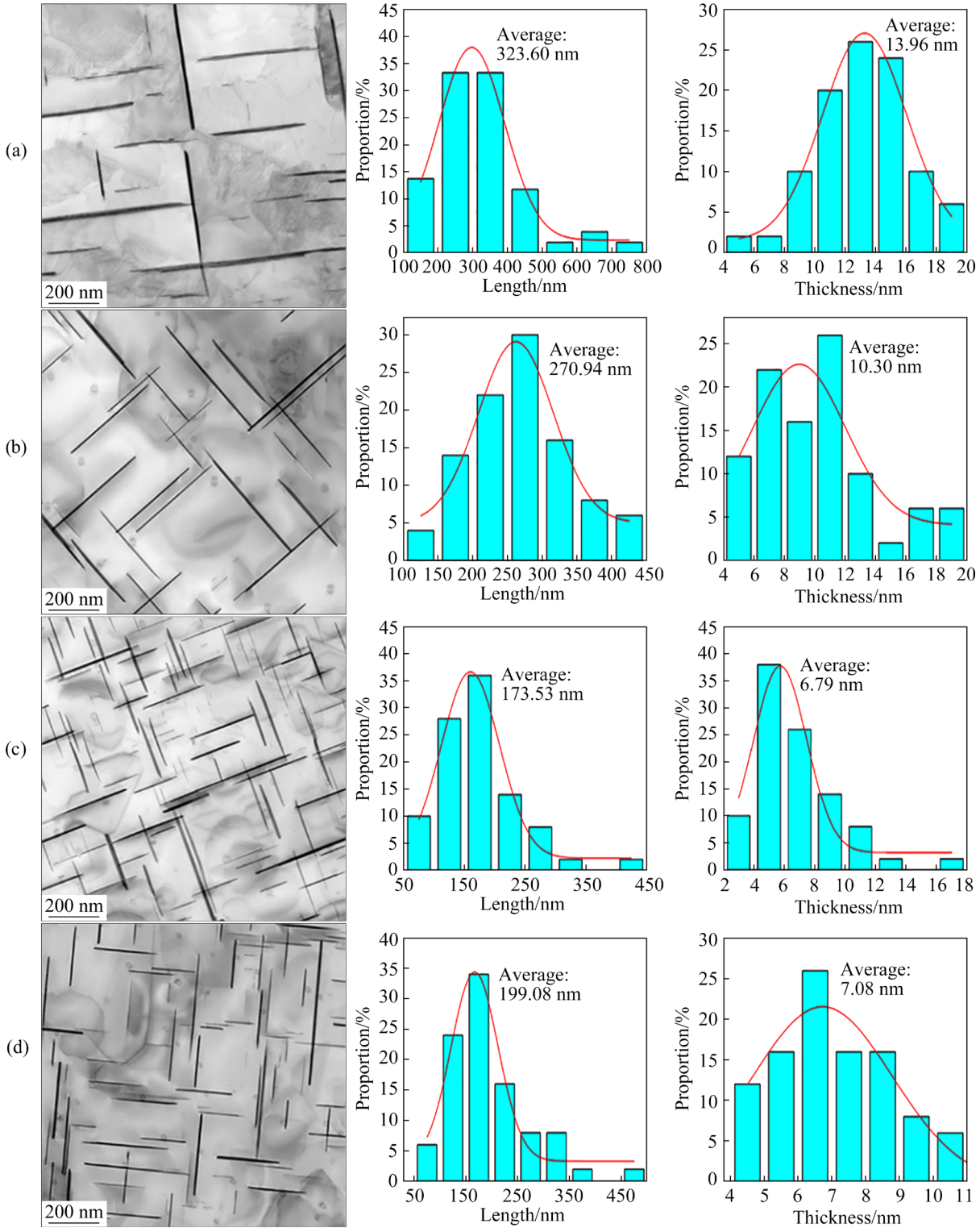

Fig. 5 TEM bright-field images of alloys after thermal exposure at 225 °C for 150 h, and corresponding length and thickness of θ' plates: (a) Al−Cu−Si; (b) Al−Cu−Er−Si; (c) Al−Cu−Er−Sc−Si; (d) Al−Cu−Sc−Si

The average length of the Al−Cu−Si alloy increased by only 9%, which was mainly due to the segregation of Mn at 300 °C at the semi-coherent interface of the θ' plates, which improved its anti-coarsening ability [12,13]. However, it is evident that the low number density of the Al−Cu−Si alloy led to weak precipitation strengthening. With the addition of Sc, the number density of the Al−Cu−Sc−Si alloy increased significantly, and the average length and thickness

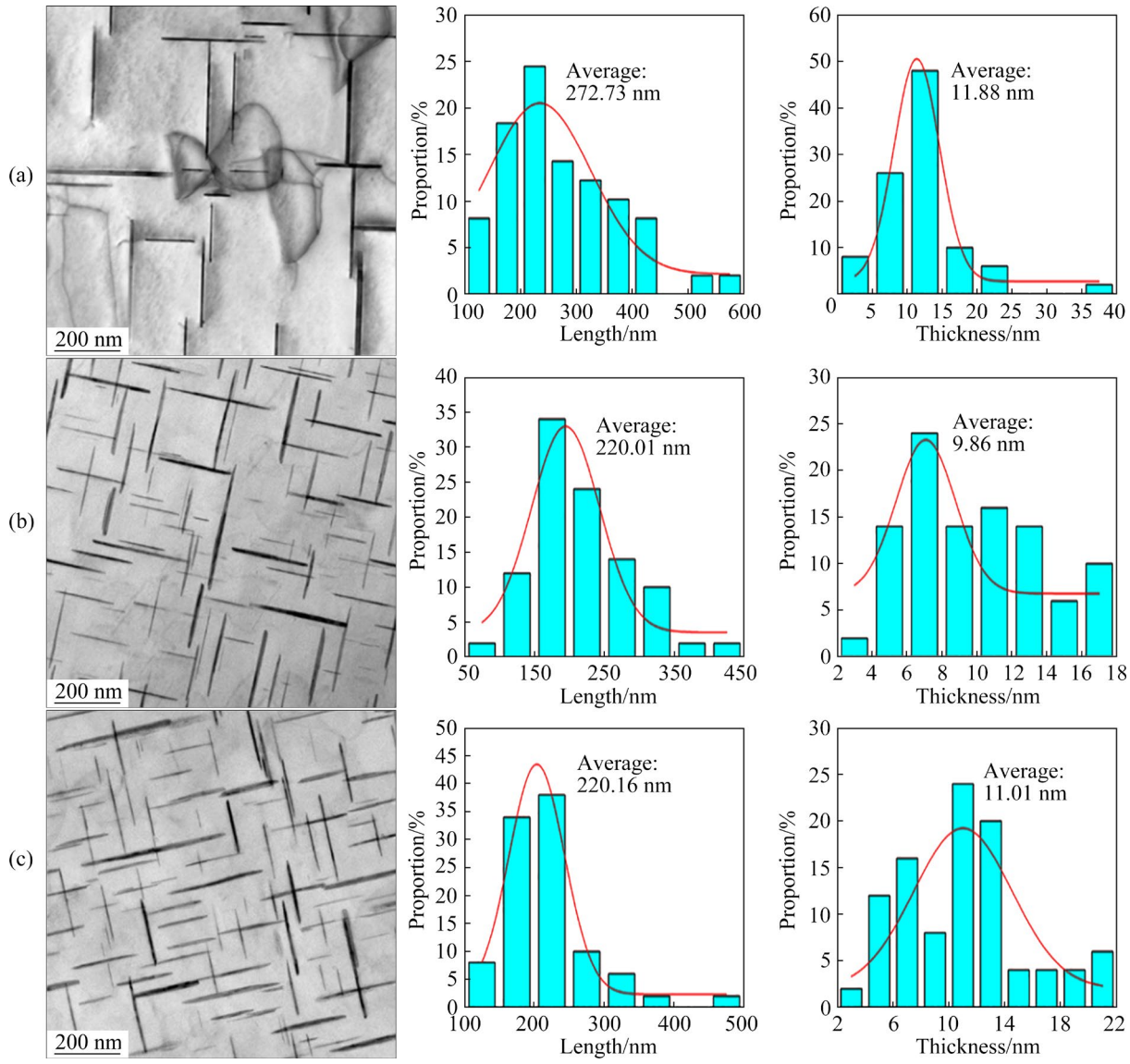

Fig. 6 TEM bright-field images of alloys after thermal exposure at 300 °C for 150 h, and corresponding length and thickness of θ' plates: (a) Al−Cu−Si; (b) Al−Cu−Er−Sc−Si; (c) Al−Cu−Sc−Si

increased by 29% and 86%, respectively. With the further co-addition of Er and Sc, thermal exposure at the same temperature caused increase of only 22% in length and 60% in thickness. The results clearly show that the co-addition of Er and Sc can improve the coarsening resistance of θ' plates in Al−Cu alloy at high temperatures.

4 Discussion

4.1 Precipitation of ordered $L1_2$ and θ' precipitates with addition of Er and Sc

The addition of Si to Al−Cu−Sc alloy significantly increases the age-hardening of the alloys after artificial aging at 175 °C. The hardness of Al−Cu alloys is mainly related to the number density, volume fraction, and aspect ratio of θ' precipitates in the Al-matrix. Higher number densities and greater maximum aspect ratios of θ' precipitates can better disrupt dislocation motion during stress, thereby increasing the hardness of the alloy [30]. The diffraction patterns from the peak-aged Al−Cu−Er−Sc−Si and Al−Cu−Sc−Si alloys (aged at 175 °C for 12 h) along the $[001]_{Al}$ zone axis of the matrix contain superlattice reflection corresponding to $L1_2$ ordering and reflection of θ' phases (Figs. 3(c, d)). BOOTH-MORRISON et al [26] found that the alloy with added Si had larger number density and volume fraction of precipitates than the Si-free alloy, which could explain the

higher peak hardness in the Al−Cu−Sc alloy with added Si. The addition of Si accelerated the Er and Sc diffusion kinetics and increased the driving force for $L1_2$ precipitation. Si−vacancy−Sc clusters could potentially form during the pre-aging at 400 °C, and these could later act as the nucleation sites for the $L1_2$ precipitates. The binding of Si to Sc atoms reduces both the vacancy formation energy in the vicinity of Sc and the Sc migration energy in Al, which further accelerates the precipitation kinetics of the $L1_2$ precipitates [31,32]. The preferential nucleation of θ' plates on the $L1_2$-ordered precipitates in the matrix can decrease the size of the precipitates and make them uniformly distributed, which results in more significant precipitate strengthening. Similar observations have been reported in previous studies. For example, $L1_2$-ordered $(Al,Cu)_3(Zr,Ta)$ precipitates in Al−2Cu−0.15Zr−0.12Ta have been shown to act as precipitation sites for Cu-enriched θ' and θ'' plates [20]. POPLAWSKY et al [12] found that the $L1_2$ precipitate exhibited a mixture of Ti and Zr on the *B* sites, with a higher Zr content ($Al_3(Zr_x,Ti_{1-x})$). BANSAL et al [22] reported that the $(Al,Si)_3Hf$ precipitated phase and the θ''/θ' plates have a synergistic coupling effect on enhancing the strengthening effect of the precipitated phase.

HAADF-STEM mapping was used to characterize the $L1_2$-ordered precipitates and θ' plates. Figures 7 and 8 show the EDS composition maps of the Al−Cu−Er−Sc−Si and Al−Cu−Sc−Si alloys after artificial aging at 175 °C for 12 h, respectively. The pre-existing $L1_2$-ordered spherical precipitates (marked with yellow arrows) were randomly distributed. Some of the spherical precipitates provide additional nucleation sites for the precipitation of θ' plates and refine the size. Moreover, some of the spherical precipitates are in broad faces in contact with the θ' plates, resulting in lower interfacial coherent strains. Thus, a high number density of θ' plates can be seen in the matrix. According to the EDS mapping results, the elemental distribution of the θ' plates did not exhibit partitioning of Si, Er, Sc, and Mn. The spherical dispersions were, instead, found to be rich in Sc and Zr, with no detectable Si, Mn, or Cu. We confirmed that the spherical dispersion was an $Al_3(Sc,Zr)$ precipitate with a core-shell structure.

Direct aging at 400 °C prior to the solid solution treatment has been reported to pre-precipitate $L1_2$-ordered precipitates. LIU et al [24] and BOOTH-MORRISON et al [25] found that the addition of Er significantly improved the hardness of Al−Sc−Zr alloys, with the effect being

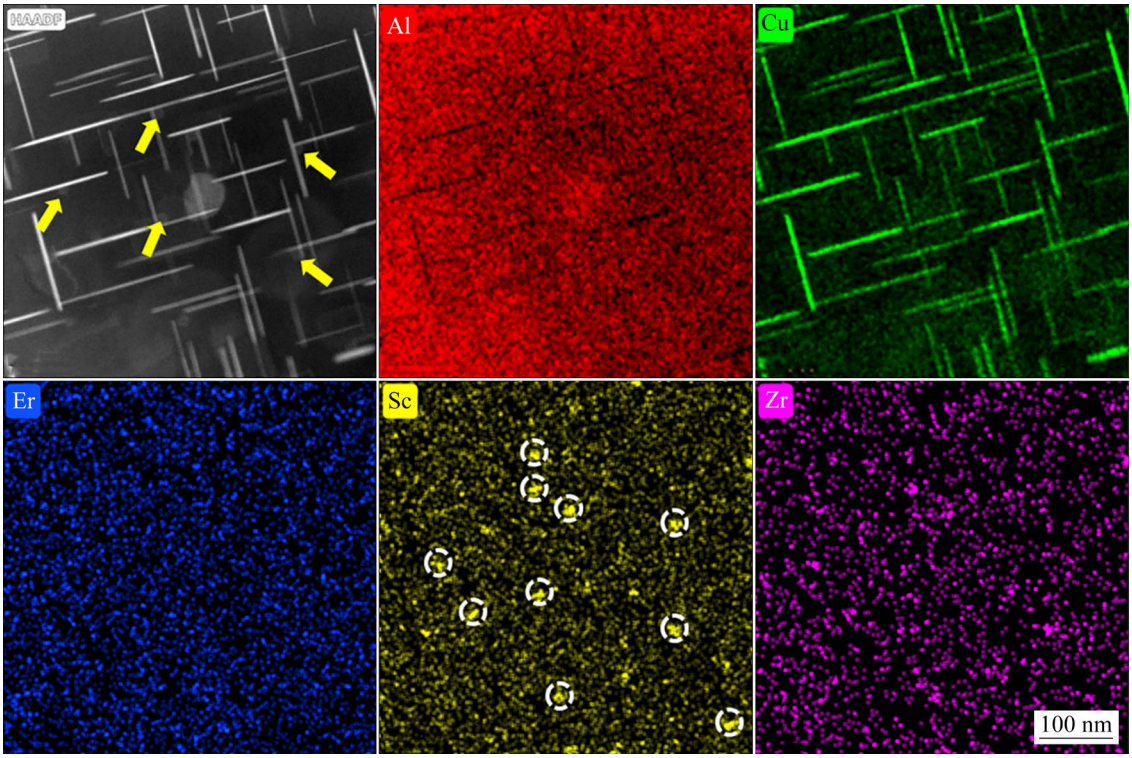

Fig. 7 HAADF-STEM micrograph and corresponding EDS maps of Al, Cu, Er, Sc and Zr for Al−Cu−Er−Sc−Si alloy after treatment at 175 °C for 12 h

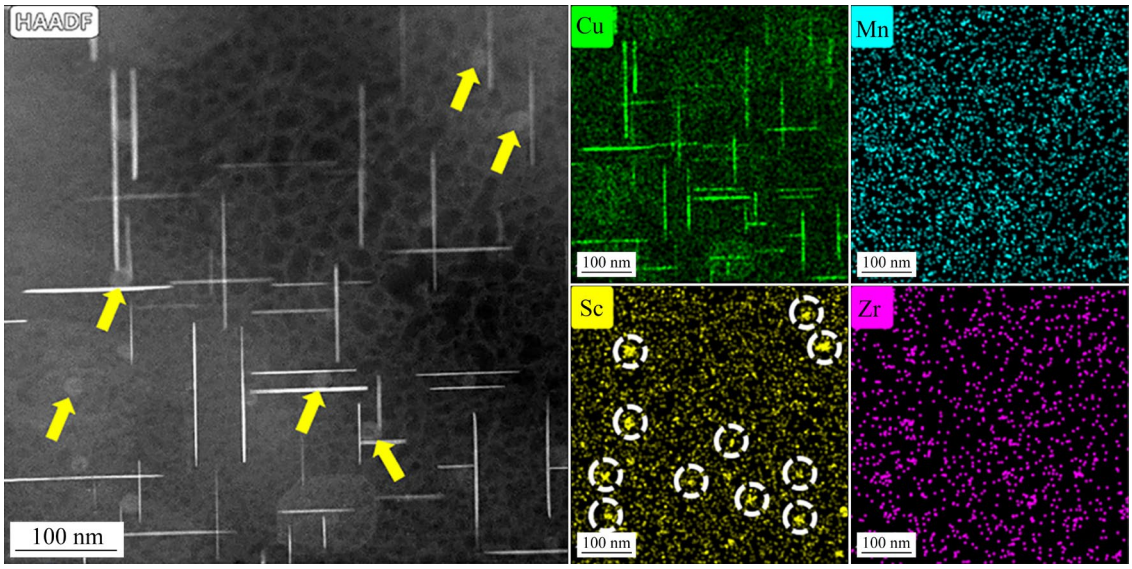

Fig. 8 HAADF-STEM micrograph and corresponding EDS maps of Cu, Mn, Sc and Zr for Al−Cu−Sc−Si alloy after treatment at 175 °C for 12 h

more obvious for aging at 400 °C. The density of $L1_2$-structure nanoparticles was higher and the dispersion was uniform. Only a limited number of Sc atoms remained in the solid solution due to the early precipitation of the Al_3(Sc,Zr) dispersion. In addition, the Zr-rich shell acts as a dynamic diffusion barrier, causing the majority of Sc atoms to be intercepted. As a result, we did not detect segregation of Sc at the θ' precipitate interface. Similarly, Mn and Zr did not segregate at the interface of the θ' precipitates. This can be mainly explained by the low mobility of Mn and Zr at 175 °C. The addition of Er to Al−Sc binary alloys was reported to accelerate the precipitation of $L1_2$ structures [24], but this was not observed in our work. Surprisingly, we found that the addition of Er resulted in a slight decrease in the size of the Al_3(Sc,Zr) dispersion. The co-addition of Er and Sc also improved the coarsening resistance ability of the θ' precipitates during subsequent thermal exposure at 225 and 300 °C.

4.2 Synergistic effect of Er and Sc stabilizing coarsening of θ' phase

The synergistic effect of Er and Sc was found to improve the coarsening resistance of θ' precipitates in Al−Cu alloys at elevated temperatures, as a comparison of the hardness results showed that the hardness values of Al−Cu−Si and Al−Cu−Sc−Si alloys were more destabilized at 225 and 300 °C. As described above, it is the formation of Al_3(Sc,Zr) particles that promote the precipitation of the θ' phase, and there is no significant difference in the number density of the θ' phase between the Al−Cu−Er−Sc−Si and the Al−Cu−Sc−Si alloys. However, the corresponding statistical results for the length and thickness of θ' precipitates showed that these parameters were slightly decreased in the Al−Cu−Er−Sc−Si alloy matrix compared to those in the Al−Cu−Sc−Si alloy matrix after thermal exposure at 225 and 300 °C for 150 h.

HAADF-STEM mapping analyses show that after exposing the artificially aged Al−Cu−Er−Sc−Si and Al−Cu−Sc−Si alloys to a temperature of 225 °C for 150 h, only Er is enriched around or inside the θ' plates, as indicated by the white dashed lines in Fig. 9(a). This indicates that the segregation of Er in the θ' precipitate helps to improve the interfacial stability of the coherent Cu-rich θ'/α-Al. When the temperature is increased to 300 °C, the hardness values of Al−Cu−Er−Sc−Si and Al−Cu−Sc−Si alloys decrease rapidly in the early stage of aging (see Fig. 2(b)), which may be related to rapid coarsening of the θ' precipitates. CHEN et al [33] studied the coarsening kinetics of the θ' phase and found that the Liftshitz−Slyozov−Wagner (LSW) coarsening model is the dominant coarsening mechanism for the θ' precipitates in the temperature range of 230−320 °C. A modified coarsening equation for the precipitation kinetics of the discoidal phase can be expressed as follows:

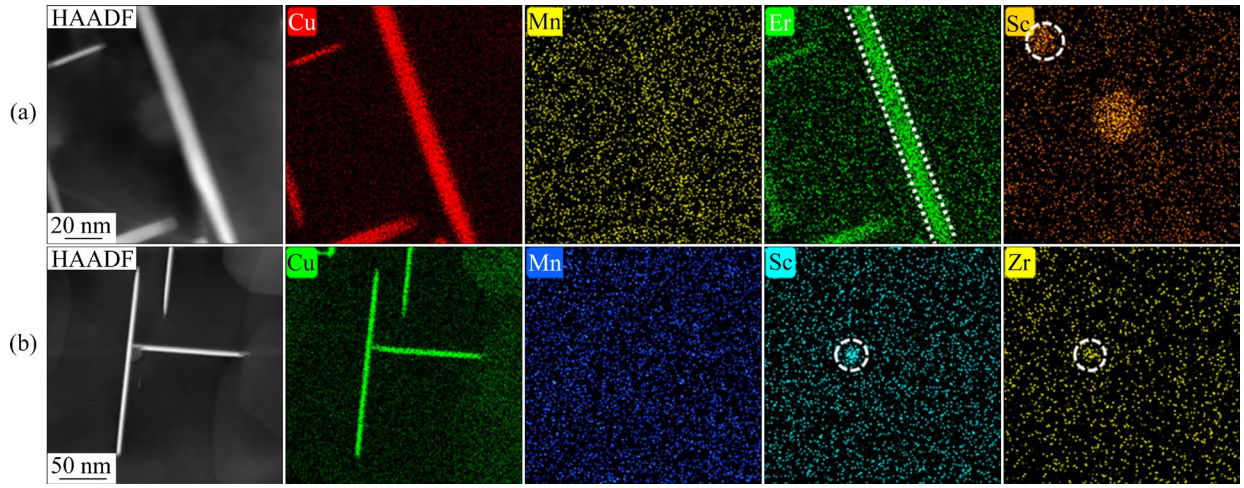

Fig. 9 HAADF-STEM micrograph and corresponding EDS maps of Cu, Mn, Er, Sc, and Zr for alloys after thermal exposure at 225 °C for 150 h: (a) Al−Cu−Er−Sc−Si; (b) Al−Cu−Sc−Si

$$d_2^3 - d_1^3 = K \cdot (t_2 - t_1) \quad (1)$$

where the rate constant K depends on the temperature as per the Arrhenius relationship, and d_1 and d_2 are the average precipitate diameters at time t_1 and t_2, respectively. The coarsening rate increases with increasing aging temperature. The higher solubility and diffusion rate of the Cu solute atoms in the Al matrix at 300 °C result in a lower activation energy for the coarsening of the θ' precipitates. Thus, the θ' precipitates coarsen rapidly. Additionally, interfacial segregation depends on kinetic factors such as solute diffusivity. The diffusion rates of the Er and Sc solute atoms are increased, but are slower compared with that of Cu solute atoms (D_{Er}=(4±2)×10^{-19} m^2·s^{-1} at 300 °C [34]). They cannot effectively segregate to θ'/α-Al interface, and thus do not act as a barrier for the diffusion of Cu atoms in the early stage of 300 °C thermal exposure. Therefore, a decrease in the HV was observed during the initial few hours (~4 h).

The relatively rapid diffusion of Er solute atoms in the Al matrix is closely related to vacancies. The high diffusion rate of Er corresponds to the strong binding energy (~0.1 eV) between Er atoms and vacancies [24]. The bond energy between Er atoms and vacancies is higher than that of Sc vacancy binding. Due to the high diffusivity and the strong attraction between Er atoms, the presence of Er atoms in the matrix can combine with more vacancies by forming Er vacancy clusters, The Er atoms in the Er vacancy clusters can remain in the θ' structure after thermal exposure at 300 °C. A similar vacancy mechanism has been reported [26,35]. NIU et al [15] proposed the substitution of Ce for coherent Cu-rich θ'/α-Al interface. After Ce substitution, the Cu-rich θ'/α-Al interface is more stable, which makes the movement of interstitial Cu atoms relatively difficult; thus, the θ' phase is more stable. Our results also indicate the segregation of Er in the θ' precipitates. In short, the addition of Er further stabilizes the θ' phase at higher temperatures.

Interestingly, the HAADF-STEM results demonstrated that the elements Sc and Mn were enriched around the θ' particles after 300 °C thermal exposure, as shown in Fig. 10. The distribution of Sc was similar to that of Mn. However, the distributions of Sc and Mn around the θ' particles were not uniform, in sharp contrast to the uniform distribution of Er. Mn was more likely to segregate at the semi-coherent interface of θ' in the Al−Cu−Mn−Zr alloy. The segregation of a large number of Mn solute atoms at the semi-coherent interface may inhibit that of Sc to the semi-coherent interface, resulting in easier segregation of Sc solute atoms at the coherent interface. Therefore, during thermal exposure at 300 °C, Sc and Mn atoms are enriched in front of the θ'/α-Al interface, forming a Sc/Mn-rich layer, which further hinders the coarsening of θ' at higher temperatures. The diffusion rates of Sc and Mn in Al solution are slower than that of Er. Therefore, Sc and Mn cannot diffuse to the θ' interface at low temperature in a short time, which explains the rapid decrease in the

hardness of Al−Cu−Sc−Si alloy in the early stage of 225 °C thermal exposure.

As the thermal exposure time increases, the hardness gradually tends to decrease, indicating that more Sc and Mn solute atoms begin to segregate at the θ'/α-Al interface and stabilize the θ' precipitate. The diffusion rates of the Sc and Mn atoms increase at 300 °C [13,25] (D_{Sc}=9.1×10^{-20} m^2·s^{-1}, and D_{Mn}=7.03×10^{-22} m^2·s^{-1} at 300 °C). Although the segregation of Sc and Mn elements at the θ'/α-Al interface was also observed in the Al−Cu−Sc−Si alloy (Fig. 11), the θ' plate rapidly coarsened, as shown in Fig. 6. The Er solute atoms are preferentially enriched in the θ' plates, which provides thermal stability for θ' and inhibits the rapid coarsening of the θ' microstructure in the early stage of thermal exposure. Thus, elements with slow diffusion rates, such as Sc and Mn have sufficient time to segregate to the θ' interface. Without the addition of Er, the combination of Sc and Mn cannot effectively stabilize the θ' plate. This is not the first report in which elements with

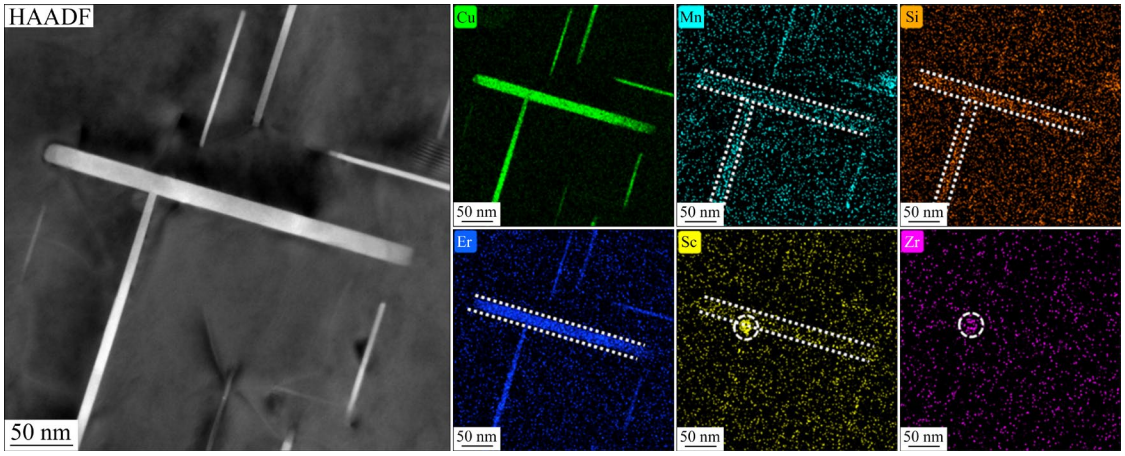

Fig. 10 HAADF-STEM micrograph and corresponding EDS maps of Cu, Mn, Si, Er, Sc and Zr for Al−Cu−Er−Sc−Si alloy after thermal exposure at 300 °C for 150 h

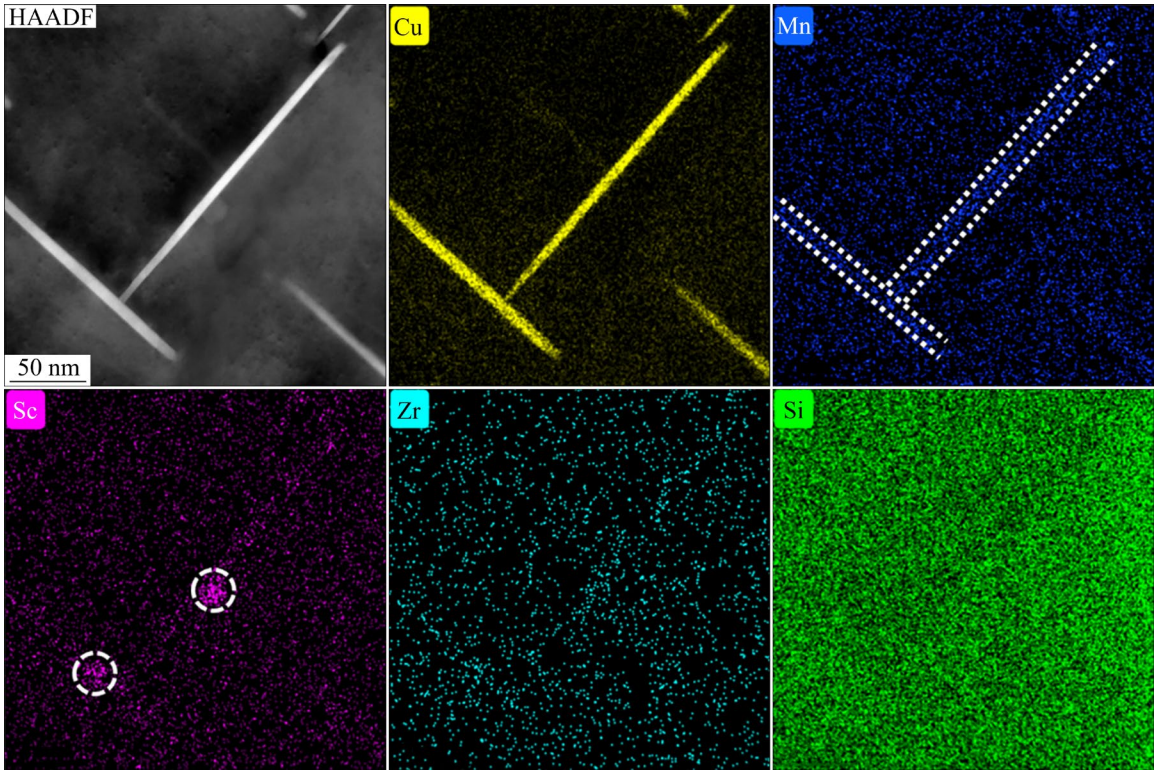

Fig. 11 HAADF-STEM micrograph and corresponding EDS maps of Cu, Mn, Sc, Zr and Si for Al−Cu−Sc−Si alloy after thermal exposure at 300 °C for 150 h

slow diffusion to the θ' interface have been used to increase the stability of the microstructure. POPLAWSKY et al [12] reported the cooperative use of Mn, Zr and Ti to increase the service temperature to 350 °C.

Based on the above analysis, the segregation of Er in the θ' structure in the early stage of thermal exposure helps to form a stable intermediate interface, which improves the microstructure stability of Al−Cu−Er−Sc−Si alloy at 225 °C. With further increase in exposure temperature, Sc and Mn play a relay role, segregating at the coherent and semi-coherent interface of θ', which hinders the coarsening of the θ' particles during high temperature thermal exposure. Therefore, the strength of the Al−Cu−Er−Sc−Si alloy after thermal exposure is much higher than that of the Al−Cu−Sc alloy.

5 Conclusions

(1) The co-addition of Er and Sc significantly accelerates age-hardening kinetics and improved the peak hardness (HV ~28.2) of the Al−Cu−Si alloy. This is attributed to the fact that the pre-existing Al_3(Sc,Zr) provides nucleation sites for the precipitation of θ' plates, stimulating their preferential nucleation. The fine distribution of θ' plates can explain the increased hardness of the Al−Cu−Er−Sc−Si alloy.

(2) Due to the significant difference in the diffusion rates of the elements Er, Sc and Mn, the Er solute atoms are preferentially enriched in the θ' plates, which inhibits the diffusion of Cu atoms and stabilizes the coarsening of θ' in the early stage of thermal exposure (225 °C).

(3) In the high-temperature (300 °C) or long thermal exposure processes, the slow diffusing elements Sc and Mn have sufficient time to segregate to the θ' coherent interface and semi-coherent interface. This interface segregation greatly reduces the interface energy and nucleation energy barrier, thus further enhancing the structural stability of the θ' plates.

CRediT authorship contribution statement

Xing-kai HOU: Investigation, Formal analysis, Data curation, Validation, Writing − Original draft, Writing − Review & editing; **Sheng-ping WEN:** Conceptualization, Supervision, Project administration, Funding acquisition; **Peng QI**, **Wu WEI**, **Xiao-lan WU**, **Hui HUANG**, **Kun-yuan GAO** and **Xiang-yuan XIONG:** Formal analysis; **Zuo-ren NIE:** Supervision, Project administration, Funding acquisition.

Declaration of competing interest

The authors declare that they have no known competing financial interests or personal relationships that could have appeared to influence the work reported in this paper.

Acknowledgments

This study is supported by the National Key Research and Development Program of China (Nos. 2021YFB3700902, 2021YFB3704204, 2021YFB3704205), Innovative Research Group Project of the National Natural Science Foundation of China (No. 51621003), Beijing Natural Science Foundation, China (No. 2202009), Basic Research Program of Jiangsu Province, China (No. BK20191148), Beijing Lab Project for Modern Transportation Metallic Materials and Processing Technology, China, and Jiangsu Key Laboratory for Clad Materials, China (No. BM2014006).

References

[1] MILLER W S, ZHUANG L, BOTTEMA J, WITTEBROOD A J, de SMET P, HASZLER A, VIEREGGE A. Recent development in aluminium alloys for the automotive industry [J]. Materials Science and Engineering: A, 2000, 280: 37−49.

[2] RAKHMONOV J U, BAHL S, SHYAM A, DUNAND D C. Cavitation-resistant intergranular precipitates enhance creep performance of θ'-strengthened Al−Cu based alloys [J]. Acta Materialia, 2022, 228: 117788.

[3] CHISHOLM M F, SHIN D, DUSCHER G, OXLEY M P, ALLARD L F, POPLAWSKY J D, SHYAM A. Atomic structures of interfacial solute gateways to θ' precipitates in Al−Cu alloys [J]. Acta Materialia, 2021, 212: 116891.

[4] BELLÓN B, HAOUALA S, LLORCA J. An analysis of the influence of the precipitate type on the mechanical behavior of Al−Cu alloys by means of micropillar compression tests [J]. Acta Materialia, 2020, 194: 207−223.

[5] LI Guang-jing, PAN Xing-hui, LIAO Heng-cheng, ZHENG Ji-wei, YANG Mo-tong, QIAN Long-jie, LU Li-zhen. Sn-induced phase transformation mechanism from θ' to θ in Al−4Cu alloy and its influence on high temperature strength [J]. Transactions of Nonferrous Metals Society of China, 2023, 33: 2559−2573.

[6] ROY S, ALLARD L F, RODRIGUEZ A, PORTER W D, SHYAM A. Comparative evaluation of cast aluminum alloys for automotive cylinder heads: Part I. Microstructure evolution [J]. Metallurgical and Materials Transactions A, 2017, 48: 2529−2542.

[7] MILLIGAN B K, ROY S, HAWKINS C S, ALLARD L F, SHYAM A. Impact of microstructural stability on the creep behavior of cast Al−Cu alloys [J]. Materials Science and Engineering: A, 2020, 772: 138697.

[8] WILLIAMS J C, STARKE E A. Progress in structural materials for aerospace systems [J]. Acta Materialia, 2003, 51: 5775−5799.

[9] SHIN D, SHYAM A, LEE S, YAMAMOTO Y, HAYNES J A. Solute segregation at the Al/θ'-Al_2Cu interface in Al−Cu alloys [J]. Acta Materialia, 2017, 141: 327−340.

[10] GAO Y H, CAO L F, KUANG J, SONG H, LIU G, ZHANG J Y, SUN J. Solute repositioning to tune the multiple microalloying effects in an Al−Cu alloy with minor Sc, Fe and Si addition [J]. Materials Science and Engineering: A, 2021, 803: 140509.

[11] YANG C, ZHANG P, SHAO D, WANG R H, CAO L F, ZHANG J Y, LIU G, CHEN B A, SUN J. The influence of Sc solute partitioning on the microalloying effect and mechanical properties of Al−Cu alloys with minor Sc addition [J]. Acta Materialia, 2016, 119: 68−79.

[12] POPLAWSKY J D, MILLIGAN B K, ALLARD L F, SHIN D, SHOWER P, CHISHOLM M F, SHYAM A. The synergistic role of Mn and Zr/Ti in producing $\theta'/L1_2$ co-precipitates in Al−Cu alloys [J]. Acta Materialia, 2020, 194: 577−586.

[13] SHYAM A, ROY S, SHIN D, POPLAWSKY J D, ALLARD L F, YAMAMOTO Y, MORRIS J R, MAZUMDER B, IDROBO J C, RODRIGUEZ A, WATKINS T R, HAYNES J A. Elevated temperature microstructural stability in cast AlCuMnZr alloys through solute segregation [J]. Materials Science and Engineering: A, 2019, 765: 138279.

[14] SUN Teng-teng, GENG Ji-wei, BIAN Ze-yu, WU Yi, WANG Ming-liang, CHEN Dong, MA Nai-heng, WANG Hao-wei. Enhanced thermal stability and mechanical properties of high-temperature resistant Al−Cu alloy with Zr and Mn micro-alloying [J]. Transactions of Nonferrous Metals Society of China, 2022, 32: 64−78.

[15] NIU Guo-dong, ZHU Lang-jie, REN Wang-rui, WANG Yu, CHEN Hou-wen, WANG Jian-feng, MAO Jian. Elevated temperature microstructural stability in Al−7Cu−0.5Mn−0.2Zr alloys through Ce addition: Enhanced coherent interfacial stability of Cu-rich θ'/α-Al interface [J]. Materials Characterization, 2023, 200: 112908.

[16] LIANG S S, MA J R, GUO K H, WEN S P, WEI W, WU X L, HUANG H, GAO K Y, LIU B S, XIONG X Y, NIE Z R. Effect of Er and Si co-microalloying on mechanical properties and microstructures of AlCuMg alloys [J]. Journal of Materials Research and Technology, 2023, 24: 430−439.

[17] CHEN B A, LIU G, WANG R H, ZHANG J Y, JIANG L, SONG J J, SUN J. Effect of interfacial solute segregation on ductile fracture of Al−Cu−Sc alloys [J]. Acta Materialia, 2013, 61: 1676−1690.

[18] RAJU P N, RAO K S, REDDY G M, KAMARAJ M, RAO K P. Microstructure and high temperature stability of age hardenable AA2219 aluminium alloy modified by Sc, Mg and Zr additions [J]. Materials Science and Engineering: A, 2007, 464: 192−201.

[19] JIANG L, ROUXEL B, LANGAN T, DORIN T. Coupled segregation mechanisms of Sc, Zr and Mn at θ' interfaces enhances the strength and thermal stability of Al−Cu alloys [J]. Acta Materialia, 2021, 206: 116634.

[20] BANSAL U, SINGH M P, SINHA S K, SAHU D K, MONDOL S, MAKINENI S K, PAUL A, CHATTOPADHYAY K. Strength and stability through variable micro segregation behaviour of Ta and Zr solutes at intermetallic interfaces in Al−Cu alloys [J]. Acta Materialia, 2023, 259: 119254.

[21] MAKINENI S K, SUGATHAN S, MEHER S, BANERJEE R, BHATTACHARYA S, KUMAR S, CHATTOPADHYAY K. Enhancing elevated temperature strength of copper containing aluminium alloys by forming $L1_2$ Al_3Zr precipitates and nucleating θ'' precipitates on them [J]. Scientific Reports, 2017, 7: 11154.

[22] BANSAL U, SINGH M P, MONDOL S, SINHA S K, MAKINENI S K, PAUL A, KAMANIO C. The interplay of precipitation of ordered compounds and interfacial segregation in Al−Cu−Hf−Si alloys for high-temperature strength [J]. Acta Materialia, 2022, 240: 118355.

[23] de LUCA A, DUNAND D C, SEIDMAN D N. Microstructure and mechanical properties of a precipitation strengthened Al−Zr−Sc−Er−Si alloy with a very small Sc content [J]. Acta Materialia, 2018, 144: 80−91.

[24] LIU Li, JIANG Jian-tang, CUI Xiang-yuan, ZHANG Bo, ZHEN Liang, RINGER S P. Correlation between precipitates evolution and mechanical properties of Al−Sc−Zr alloy with Er additions [J]. Journal of Materials Science & Technology, 2022, 99: 61−72.

[25] BOOTH-MORRISON C, DUNAND D C, SEIDMAN D N. Coarsening resistance at 400 °C of precipitation-strengthened Al−Zr−Sc−Er alloys [J]. Acta Materialia, 2011, 59: 7029−7042.

[26] BOOTH-MORRISON C, MAO Z, DIAZ M, DUNAND D C, WOLVERTON C, SEIDMAN D N. Role of silicon in accelerating the nucleation of $Al_3(Sc,Zr)$ precipitates in dilute Al−Sc−Zr alloys [J]. Acta Materialia, 2012, 60: 4740−4752.

[27] LIN J D, OKLE P, DUNAND D C, SEIDMAN D N. Effects of Sb micro-alloying on precipitate evolution and mechanical properties of a dilute Al−Sc−Zr alloy [J]. Materials Science and Engineering: A, 2017, 680: 64−74.

[28] LIN J D, SEIDMAN D N, DUNAND D C. Improving coarsening resistance of dilute Al−Sc−Zr−Si alloys with Sr or Zn additions [J]. Materials Science and Engineering: A, 2019, 754: 447−456.

[29] ROUXEL B, RAMAJAYAM M, LANGAN T J, LAMB J, SANDERS P G, DORIN T. Effect of dislocations, $Al_3(Sc,Zr)$ distribution and ageing temperature on θ' precipitation in Al−Cu−(Sc)−(Zr) alloys [J]. Materialia, 2020, 9: 100610.

[30] NIE J F, MUDDLE B C. Microstructural design of high-strength aluminum alloys [J]. Journal of Phase Equilibria, 1998, 19: 543−551.

[31] PENG J, BAHL S, SHYAM A, HAYNES J A, SHIN D. Solute-vacancy clustering in aluminum [J]. Acta Materialia, 2020, 196: 747−758.

[32] VO N Q, DUNAND D, SEIDMAN D N. Role of silicon in the precipitation kinetics of dilute Al−Sc−Er−Zr alloys [J]. Materials Science and Engineering: A, 2016, 677: 485−495.

[33] CHEN Zhong-wei, ZHAO Yan-ni, ZHANG Zhe. Theoretical and experimental study of precipitation and coarsening

kinetics of θ' phase in Al−Cu alloy [J]. Vacuum, 2021, 189: 110263.

[34] van DALEN M E, KARNESKY R A, CABOTAJE J R, DUNAND D C, SEIDMAN D N. Erbium and ytterbium solubilities and diffusivities in aluminum as determined by nanoscale characterization of precipitates [J]. Acta Materialia, 2009, 57: 4081−4089.

[35] DONG Ming-ye, ZHAO Yue, LI Quan, WANG Fu-de, WU Ai-ping. Effects of Cd addition in welding wires on microstructure and mechanical property of wire and arc additively manufactured Al−Cu alloy [J]. Transactions of Nonferrous Metals Society of China, 2022, 32: 750−764.

Er 和 Sc 对 Al−Cu 合金时效行为和 θ'析出稳定性的协同作用

侯兴凯[1]，文胜平[1]，亓 鹏[2]，魏 午[1]，吴晓蓝[1]，黄 晖[1]，高坤元[1]，熊湘沅[1]，聂祚仁[1]

1. 北京工业大学 工业大数据应用技术国家工程实验室 材料与制造学部，北京 100124；
2. 中国铝业科学技术研究院有限公司，北京 102209

摘 要：采用透射电子显微镜(TEM)和高角度环形暗场(HAADF)成像系统研究 Er 和 Sc 协同添加对合金时效和界面偏析行为的影响。TEM 结果表明，具有核壳结构的 $Al_3(Sc,Zr)$可以作为 θ'的形核位点促进其均匀细小析出。STEM 结果表明，在 225 ℃下热暴露 150 h 的过程中，Er 溶质原子优先富集在 θ'相结构内部。然而，在 300 ℃时观察到 Sc 和 Mn 溶质原子在 θ'/α-Al 基体界面处偏析。由于 Er 在 θ'相结构中的早期富集，缓慢扩散的 Sc 和 Mn 在 θ'相发生严重粗化之前偏析到 θ'析出相的界面处，从而在更高的温度下进一步稳定 θ'析出相。

关键词：Er−Sc 共添加；时效行为；θ'析出稳定性；溶质偏析；Al−Cu 合金

(Edited by Xiang-qun LI)